Advances in Radiation Oncology (2025) **10**, 101715

advances in radiation oncology

www.advancesradonc.org

Teaching Case

Investigating an Artificial Object Detected in Radiographic Images in a Child: Unique Considerations Related to Proton Therapy

Jiyeon Park, PhD,[a] Daniel J. Indelicato, MD,[a,*] Soon N. Huh, PhD,[a] Bobby R. Waldrip, BS, RTT,[b] Mark Artz, PhD, MBA,[a] Yawei Zhang, PhD,[a] Michael Vieceli, MS,[c] Hardev Grewal, PhD,[a] and Perry Johnson, PhD[a]

[a]Department of Radiation Oncology, University of Florida College of Medicine, Jacksonville, Florida; [b]Medical Dosimetry Program, University of Wisconsin-La Crosse, La Crosse, Wisconsin; and [c]University of Florida Health Proton Therapy Institute, Jacksonville, Florida

Received 11 July 2024; accepted 3 January 2025

Introduction

Although each patient's treatment is unique, radiation therapy for pediatric patients require close observation of symptoms and attention to anatomic changes.[1,2] Given that foreign body (FB) ingestions commonly occur in pediatric patients of all ages,[3,4] reviewing the daily radiograph images acquired during the patient's alignment is a significant index to ensure prompt patient care and robust radiation therapy. Adolescents are not exempt from FB ingestions,[5] which can occur accidentally, intentionally, or because of underlying mental illness and developmental delay.[6] If an adolescent patient does not disclose ingesting a FB, the presentation of the FB might be delayed, leading to urgent interventions, especially when the FBs are batteries, magnets, sharp objects, or superabsorbent materials.[3-5] However, if a patient with FB ingestion is asymptomatic and urgent removal is not required, a clinical decision needs to be made regarding whether radiation therapy can proceed depending on the FBs size, properties, location, and patient's medical conditions. It is important to consider potential complications and dosimetric effects on the treatment site considering FBs radiation interactions and management of the ingested FB. If proton therapy is being used because the modality of choice, considerable attention is required because of the sensitivity of protons to various uncertainties and tissue types,[7] as well as the potential dose perturbation effects.[8-10] When the FB made of high atomic number (Z) material is placed in the path of proton beams, it can lead to dose enhancement downstream because of the higher energy loss of the primary proton beams with stronger Coulomb interaction[8] and the secondary particles generated in vicinity of the object.[9] However, it can also result in a dose deficit behind the object and a range pullback at the distal end.[8,10] Such proton interactions in clinical cases may cause dose inhomogeneity in the treatment area, which can degrade the target dose coverage.[10] The degree of these effects depends on several factors, including the size, location, orientation, and material of the FB, as well as the energies, field sizes, and angles of the proton beams.

During our routine procedures, we encountered an unexpected finding of an artificial object in the daily orthogonal radiographs. Recognizing the potential implications of this discovery, we investigated whether the material's location and properties could affect the patient's treatment by causing perturbed doses to the target or adjacent tissues, compromising care. Careful considerations were given to ensuring that the object in the

Sources of support: This work had no specific funding.

Research data are stored in an institutional repository and will be shared upon request to the corresponding author.

*Corresponding author: Daniel J. Indelicato, MD; Email: dindelicato@floridaproton.org

https://doi.org/10.1016/j.adro.2025.101715

2452-1094/© 2025 The Authors. Published by Elsevier Inc. on behalf of American Society for Radiation Oncology. This is an open access article under the CC BY-NC-ND license (http://creativecommons.org/licenses/by-nc-nd/4.0/).

bowel does not interfere with proton spot delivery. We comprehensively analyzed possible materials in a phantom test to identify the FB using radiographs and cone-beam computed tomography (CBCT) projection images. Moreover, the possible dosimetric effect with the FB was evaluated, considering clinical cases that can be affected by unexpected artificial bowel contents.

Case presentation

Artificial object detected in orthogonal radiograph images during patient alignment

A 16-year-old girl pediatric patient underwent proton treatment for World Health Organization grade 2 lumbar spine myxopapillary ependymoma after laminectomy with gross total resection. Planning target volume for the first phase treatment covers from the L1 to S3 vertebrae (Fig. 1). The radiation dose was prescribed to deliver 50.4 Gy_{RBE} in 28 fractions followed by a sequential boost dose of 3.6 Gy_{RBE} in 2 fractions to L2 using the pencil-beam scanning (PBS) technique (ProteusPlus, Ion Beam Applications). Two posterior-oblique beams ($\pm$15° from a posterior beam axis) were used to avoid range uncertainties because of daily gastrointestinal organ changes and minimize bowel and kidney doses.

Orthogonal radiographs were taken using a pediatric pelvis protocol (90 kVp) to align the patient (Fig. 2a). In the coronal view of the anterior-posterior (AP) radiographs, we observed an enhanced ellipsoidal object, as shown in Fig. 2b-f. The object measured 1.5 cm by 1 cm for the major and minor axis of the ellipse. However, it was not visible in the lateral radiograph because of overlap with the L4 vertebra, which made it difficult to determine its exact depth in the abdomen. After the first AP radiograph, the patient was asked to get off the table to ensure the object was not placed on the treatment couch or the patient's gown. While repositioning the patient, as in Fig. 2c-e, we confirmed that there was no artificial object in the previous treatment fractions. An additional AP image was obtained to confirm the final patient setup after applying the correction vector following CBCT images as illustrated in Fig. 2f. We then focused on determining the location of the artificial object, its interference with the distal spot position, the patient's potential symptoms from the suspected new FB in her right lower abdominal quadrant, and the safety of proceeding with the planned treatment.

CBCT images and clinical decision for safe treatment

To better understand the object's location, we scanned CBCT images (Fig. 3a-c) using a pediatric protocol (80 kVp) with a partial arc. However, the patient- and calibration-related artifacts of CBCT images can lead to misinterpretation of anatomic changes.[11,12] Therefore, we reviewed CBCT projection images with 30 to 40 gantry angle increments (in the IEC 61217 coordinate system),[13] referring to the AP images as in Fig. 3d-i. We confirmed that the enhanced object was presented in the projection images and was not created by the CBCT artifacts.

To ensure the safe distance between the FB and the PBS spot, we registered the CBCT images alongside the CT images used for treatment planning. After confirming that the FB was situated in the bowel, the FB in the CBCT images was contoured and overlaid onto the CT images. Next, we navigated to the CT slice containing the most medial extension of the contoured FB to measure the distance to the nearest spot placement. Even when accounting for systematic uncertainties associated with the spot position and size as well as the FBs size measured in AP radiographs and the CBCT projection images, we determined that there was a safe margin of 3 cm laterally toward the patient's right side. Furthermore, to address the potential movement of the FB because of bowel peristalsis during the beam-on time, we assessed a worst-case scenario related to the FBs position at the distal end of beam. Our findings revealed that the FB in the bowel was

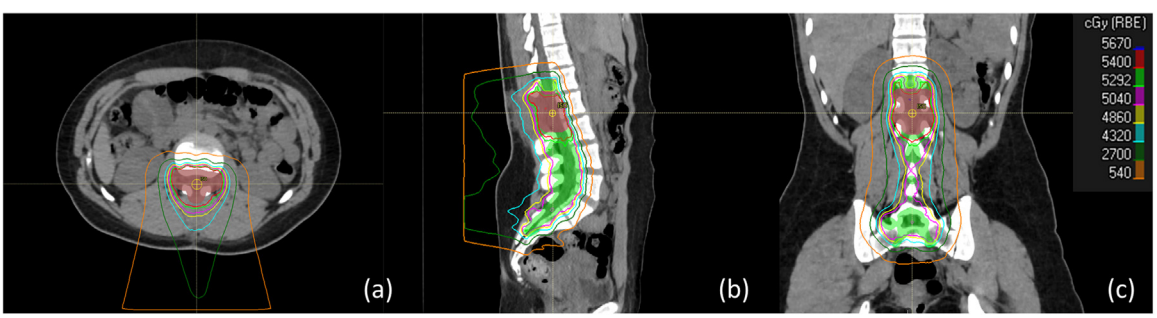

Figure 1 Composite dose distribution (54 Gy_{RBE} with a 50.4 Gy_{RBE} after a boost dose of 3.6 Gy_{RBE}) in (a) axial, (b) sagittal, and (c) coronal views for the case to be treated with 2 posterior-oblique proton beams for the spinal myxopapillary ependymomas from L1 to S3. The green and red structures represent the initial and boost target volumes, respectively.
Abbreviation: Gy_{RBE} = relative biologic effectiveness-weighted dose in gray.

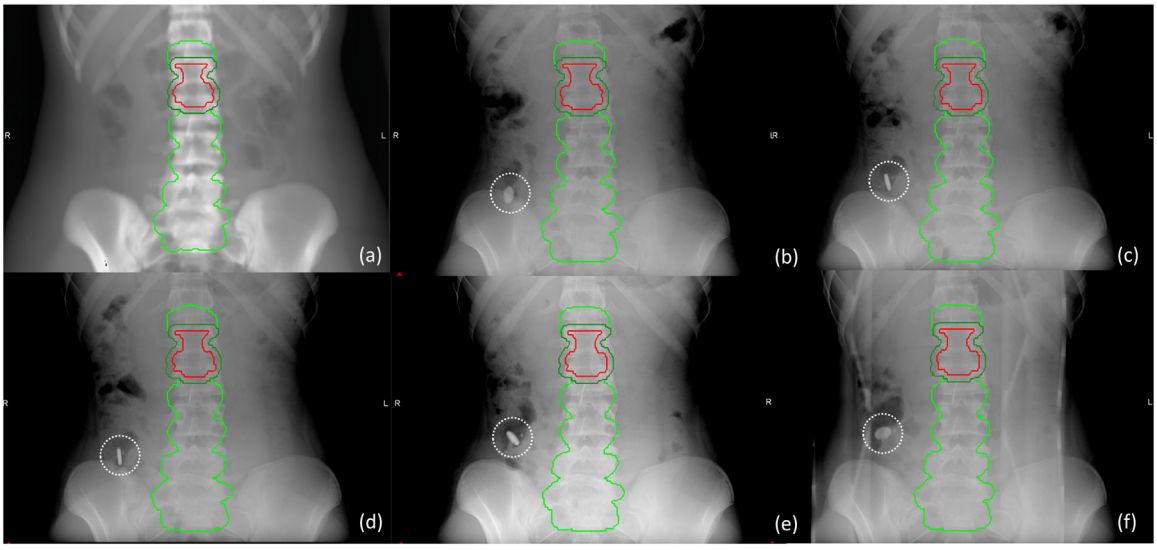

Figure 2 An artificial object detected in the AP radiographs during patient alignment. The fluorescent green color indicates the PTV for the initial treatment, delivering 50.4 Gy_{RBE}. The clinical target volume and PTV for a boost dose of 3.6 Gy_{RBE} are represented by red and green. Digitally reconstructed radiography is used as a (a) reference, whereas AP radiographs were acquired during the initial attempt of (b) patient setup and at different elapsed times of (c) 5.8 minutes, (d) 9.1 minutes, (e) 15.7 minutes, and (f) 29.6 minutes.
Abbreviations: AP = anterior-posterior; PTV = planning target volume; Gy_{RBE} = relative biologic effectiveness-weighted dose in gray.

located outside the 1% isodose line of the daily prescribed dose. The hypothetical position of the FB in the worst scenario was >1 cm away from the closest PBS spot related to the distal end of the beam, even when considering range uncertainties by a 3.5% density error related to the Hounsfield units (HU) of the patient tissues. After the radiation oncologist had reviewed the images and evaluated the situation, it was concluded that treatment could safely proceed as normal.

Patient disclosure concerning the FB and follow-up imaging

Although the patient was asymptomatic on the day of treatment, we inquired if they could recall any specifics about what they had ingested since their previous treatment. However, they could not recollect specific details, particularly concerning any radiopaque materials. We also asked their caregivers if they had witnessed the patient ingesting any unusual objects and whether this incident had occurred before, but they denied having observed such incidents. The radiation oncologist requested that they check the patient's stool in the following days, but they reported not finding anything out of the ordinary. Before the subsequent treatment, the patient's symptoms were re-evaluated and there were no remarkable changes. We confirmed that the FB had exited the patient's body through follow-up radiograph images taken on the next day of treatment.

Phantom test and dosimetric simulation in PBS treatment plan

Determining the type of material could help alleviate any medical concerns associated with the FB in the event it had remained within the patient's bowel for prolonged period. However, there are limitations to directly identifying the FB from the patient's radiograph images because of artifacts and the limited range to display the FBs details. To assist in the identification of the FB, we conducted a phantom study using various items (Table 1)[12,14-23] to reasonably infer the characteristics of the FB. Because the patient's object exhibited streak artifacts typically associated with metallic composition, we included accessible materials with high Z ranging from Aluminum (Z = 13) to Copper (Z =29), as well as tissue-equivalent materials. Radiographs and CBCT projection images of the test materials were obtained to help assess the findings from the patient's original images. We imitated the patient's pelvic area using the modular I'mRT phantom (IBA Dosimetry GmbH)[14] with removable cubic slabs and a bolus. By considering the size, shape, materials, and radiographic properties presented in radiograph images, we approximated the attributes of the object located within the patient. To explore the dose perturbation effect in proton treatment for pediatric patients with the ingested FB, we used CT images and structures from a pediatric patient with the target adjacent to the bowel. This allowed us to simulate clinical scenarios, as shown in Fig. 4, by calculating the hypothetical perturbed dose because of the inclusion of the FB in the PBS treatment plan (Raystation 2023B, RaySearch Laboratories AB). We adapted the

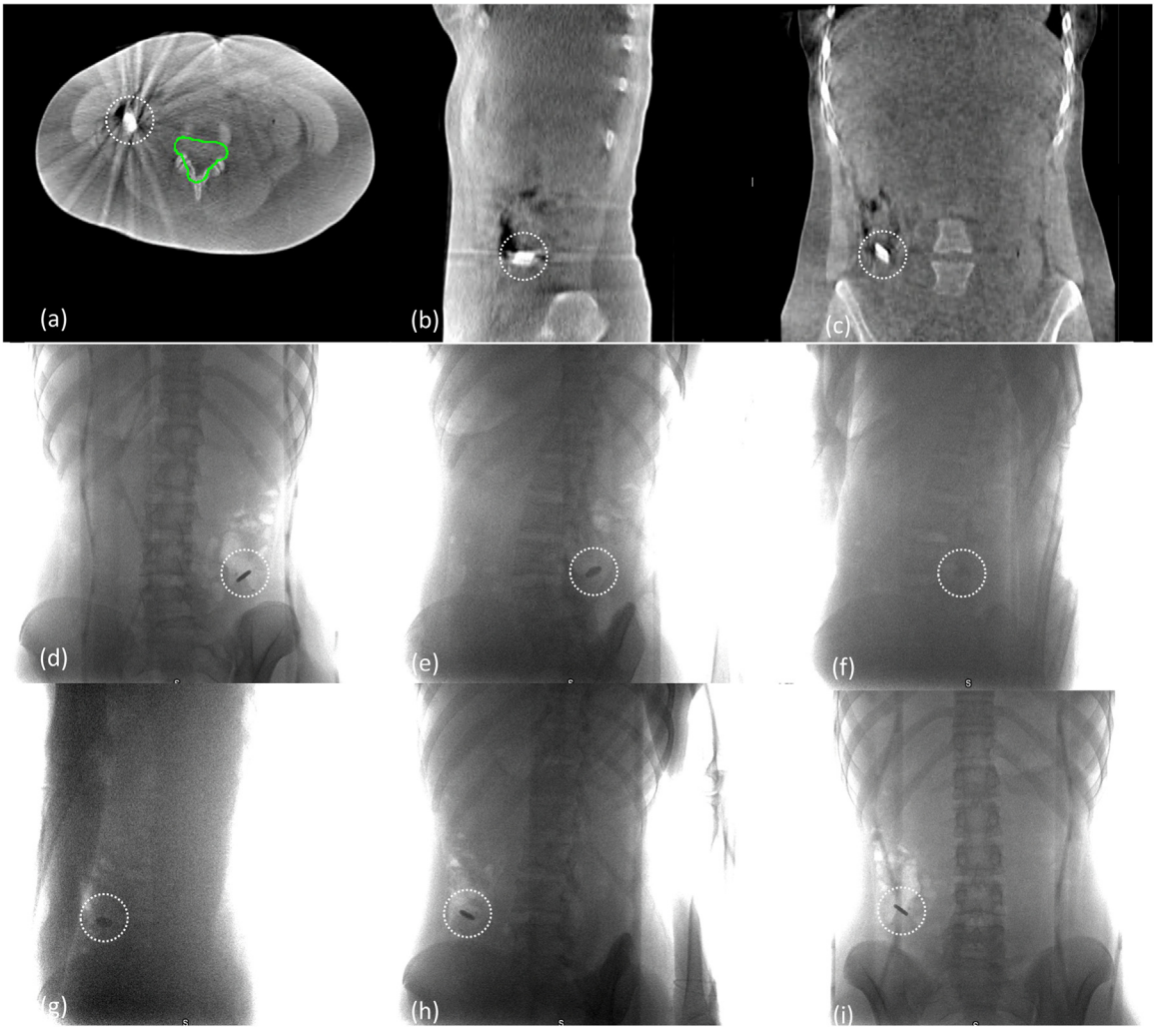

Figure 3 Raw projection and reconstructed images used to evaluate the geometric and radiological characteristics of the artificial object. The cone-beam computed tomography images show the object from (a) axial, (b) sagittal, and (c) coronal views. The radiograph tube was for the raw project images positioned at (d) 355°, (e) 325°, (f) 300°, (g) 260°, (h) 220°, and (i) 185°.

Table 1 Various items and materials tested in a pelvic phantom to identify the object detected in the radiograph images

Item	Size [mm][†]	Composition
Cubic solid water slab in the pelvic phantom[14]	160.0 × 160.0 × 10.0	RW3 [polystyrene of 98% ± titanium dioxide of 2%; $\rho = 1.045$ g/cm^3]
Acrylic disk	16.0 × 3.0	Polymethyl methacrylate [$Z_{eff} = 6.5 - 6.6$, $\rho = 1.18$ g/cm^3][15,16]
Button	15.0 × 2.0	Polyester [$Z_{eff} = 6.7$, $\rho = 1.19$ g/cm^3][16]
Household aluminum foil[17]	17.0 × 1.4	Aluminum [>98.5%; Z = 13, $\rho = 2.7$ g/cm^3] + other alloy [<1.5%]
Titanium implant [reconstruction plate][18]	96.0 × 3.0	Titanium [Z = 22, $\rho = 8.0$ g/cm^3]
Parallel pin	4.0 × 13.0	Stainless steel [$Z_{eff} = 25.5 - 26.5$, $\rho = 8.0$ g/cm^3][19,20]
Dime[21]	17.9 × 1.4	Nickel [8.33%; Z = 28, $\rho = 8.9$ g/cm^3] + copper [91.67%; Z = 29, $\rho = 8.96$ g/cm^3]
Flat washer	6.0 [ID] / 14.3 [OD] x 1.0	Brass [$Z_{eff} = 29 - 30$, $\rho = 8.4 - 8.7$ g/cm^3][22,23]

Abbreviations: mm, millimeter; Z, atomic number; Z_{eff}, effective atomic number; ρ, density; ID, inner diameter; OD, outer diameter.
†Width × length / diameter × thickness.

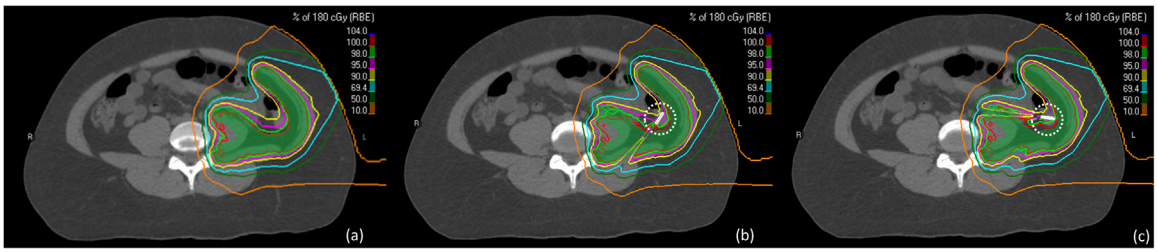

Figure 4 Proton dose perturbation by the titanium disk (18 mm in diameter and 1.4 mm thick) situated in the bowel adjacent to target in a potential clinical scenario. A comparison of the planned dose to deliver a daily prescribed dose of 1.8 Gy_{RBE} to (a) the left iliac crest, with the perturbed dose when the object is aligned to the beam at (b) 45° and (c) 95°.
Abbreviation: Gy_{RBE} = relative biologic effectiveness-weighted dose in gray.

geometric and radiographic characteristics of the object in the bowel using the phantom tests results. The dosimetric effect was assessed for a daily prescribed dose of 1.8 Gy_{RBE} to the left iliac crest, using left anterior and posterior beams at 40° and 95°.

Discussion

When we examined the patient's AP radiography over time, we noticed that a disk-shaped object moved with intestinal peristalsis for 30 minutes, as depicted in Fig. 2b-f, until the first beam was delivered. The object had its greatest displacement of 0.5 cm laterally and 2 cm in the superior-inferior direction over a 6-minute period. Although the object could be displaced the most during the beam-on time (3 minutes per field), the bowel movement of the patient case did not affect the planned dose deposition by the distal spots of the beams. The right posterior-oblique beam was chosen to be delivered first to prevent the object from moving closer to the treatment area via natural peristalsis after other beam deliveries. The object in the patient's body showed 1155.5 ± 169.5 HU greater than the HU of the vertebra body's trabecular bone (218.2 ± 83 HU). The measured HU values in the patient's CBCT images are likely to be lower than the expected HUs of the object because of the influence of the patient's organs and breathing motion. In a phantom test with various items, a dime showed a similar size, shape, and the relative enhancement ratio between the object and the surrounding tissue from the CBCT projection images, as depicted in Fig. 5. Materials with Z ≥

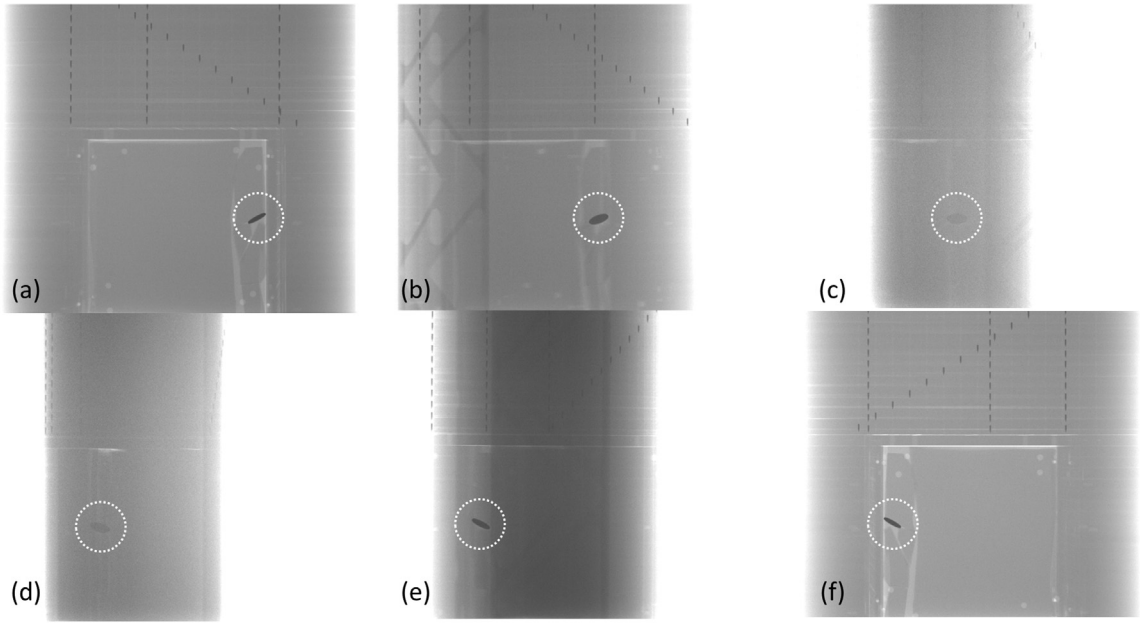

Figure 5 Raw projection images when a dime was used to estimate the artificial object in the pelvic phantom. The radiograph tube was positioned at (a) 355°, (b) 325°, (c) 300°, (d) 260°, (e) 220°, and (f) 185°.

Aluminum cannot be distinguished based on CBCTs HUs because they were saturated because of the limited dynamic range of the CBCT. When household aluminum foil was tested, it was not detectable in radiography unless it was folded and shaped to a thickness of 2 to 3 mm (1128.7 $\pm$ 153.5 HU). It barely created streak artifacts in CBCT and lacked a sturdy boundary and uniform intensity. The object appeared to be composed of a relatively high Z $\geq$ Aluminum shape solid disk based on our test results using radiographs and CBCT images.

If the FB had been found in the bowel for a clinical scenario, where the target encompasses a portion of the intestines, it is important to consider the object's short-term movement and its impact on dose during the beam-on time. For an object with a similar size to the patient's case, particularly when it has a Z $\geq$ Titanium among the tested materials in Table 1, it would be expected to cause noticeable local dosimetric changes as in Fig. 4. This effect was especially evident when the object was aligned parallel to each beam axis, leading to a remarkable dose perturbation. It resulted in a cold spot because of proton range degradation downstream of the beam and a hot spot (5%-6% higher than the planned doses) caused by the interaction with the object. Inferior local dose conformity would be expected, whereas the dose-volume histograms do not show significant changes for the target and bowel.

Conclusion

Although it involved additional exposure to diagnostic radiation, in our patient's situation, it was useful to strategically use orthogonal radiographs, CBCT, and projection images to ensure proper patient alignment and to monitor anatomic changes and identify the FB. When any artificial object that causes proton dose perturbations is found in a pediatric patient's body, extra attention is required to detect and monitor them with image guidance. Effective and timely communication between the treatment team, patient, and radiation oncologist was essential to provide safe and precise proton treatment with appropriate clinical decision-making and patient care.

Disclosures

The authors declare that they have no known competing financial interests or personal relationships that could have appeared to influence the work reported in this paper.

Acknowledgments

Jiyeon Park was responsible for statistical analysis.

References

1. Winkfield KM, Linsenmeier C, Yock TI, et al. Surveillance of craniopharyngioma cyst growth in children treated with proton radiotherapy. *Int J Radiat Oncol Biol Phys*. 2009;73:716-721.
2. Acharya S, Wang C, Quesada S, et al. Adaptive proton therapy for pediatric patients: Improving the quality of the delivered plan with on-treatment MRI. *Int J Radiat Oncol Biol Phys*. 2021;109:242-251.
3. Kramer RE, Lerner DG, Lin T, et al. Management of ingested foreign bodies in children: A clinical report of the NASPGHAN Endoscopy Committee. *J Pediatr Gastroenterol Nutr*. 2015;60:562-574.
4. Joyamaha D, Conners GP. Managing pediatric foreign body ingestions. *Mo Med*. 2015;112:181-186.
5. Sahn B, Mamula P, Ford CA. Review of foreign body ingestion and esophageal food impaction management in adolescents. *J Adolesc Health*. 2014;55:260-266.
6. Destro F, Caruso AM, Mantegazza C, et al. Foreign body ingestion in neurologically impaired children: A challenging diagnosis and management in pediatric surgery. *Children (Basel)*. 2021;8:956.
7. Paganetti H. Range uncertainties in proton therapy and the role of Monte Carlo simulations. *Phys Med Biol*. 2012;57:R99-R117.
8. Nichiporov D, Moskvin V, Fanelli L, Das IJ. Range shift and dose perturbation with high-density materials in proton beam therapy. *Nucl Instrum Methods Phys Res B*. 2011;269:2685-2692.
9. Verhaegen F, Palmans H. Secondary electron fluence perturbation by high-Z interfaces in clinical proton beams: A Monte Carlo study. *Phys Med Biol*. 1999;44:167-183.
10. Verburg JM, Seco J. Dosimetric accuracy of proton therapy for chordoma patients with titanium implants. *Med Phys*. 2013;40:071727.
11. Nagarajappa AK, Dwivedi N, Tiwari R. Artifacts: The downturn of CBCT image. *J Int Soc Prev Community Dent*. 2015;5:440-445.
12. Nelms DW, Shukla HI, Nixon E, Bayouth JE, Flynn RT. Assessment of three dead detector correction methods for cone-beam computed tomography. *Med Phys*. 2009;36:4569-4576.
13. Dicom ps3.3 2020b - Information object definitions. 8. C.8.8.25.6 coordinate systems. Accessed June 20, 2024. Https://dicom.Nema.Org/medical/dicom/2020b/output/chtml/part03/sect_c.8.8.25.6.Html.
14. IBA. Independent & integrated quality assurance for radiation therapy. Product catalog 2022. Accessed June 20, 2024. https://www.iba-dosimetry.com/fileadmin/user_upload/products/02_radiation_therapy/Product-Catalog-RT-Br-E_Rev.2_2022_09-01.pdf.
15. Hubbell JH, Seltzer SM. Tables of x-ray mass attenuation coefficients and mass energy-absorption coefficients from 1 keV to 20 meV for elements z = 1 to 92 and 48 additional substances of dosimetric interest. X-ray mass attenuation coefficients; nist standard reference database 126. Created September 17, 2009, Updated February 17, 2022. Accessed August 20, 2024. Https://dx.Doi.Org/10.18434/t4d01f.
16. Sookpeng S, Cheebsumon P, Pengpan T, Martin C. Comparison of computed tomography dose index in polymethyl methacrylate and nylon dosimetry phantoms. *J Med Phys*. 2016;41:45-51.
17. Standford Advanced Materials. Alf1462 aluminum alloy 1100 foil. Accessed June 20, 2024. https://www.samaterials.com/aluminium/1462-aluminum-alloy-1100-foil.html.
18. KLS Martin Group. Levelone fixation osteosynthesis 2.0 - 2.7 fracture and reconstruction threadlock ts. Accessed June 20, 2024. https://www.klsmartin.com/mediathek/90-442-02-04_LevelOne_Fixation_Osteosynthesis_2_0-2_7_Fracture_and_Reconstruction_Threadlock_TS.pdf.

19. Rajamanickam T, Muthu S, Murugan P, et al. Studies on fundamental interaction parameters for stainless steel and titanium biomaterials using flattened and un-flattened mega-voltage x-ray beams. *Asian Pac J Cancer Prev*. 2019;20:2485-2491.
20. Vegas Fastener Manufacturing. Stainless steel 316. Accessed June 20, 2024. Https://www.Vegasfastener.Com/materials/stainless-steel-316/.
21. United States Mint. Coin specifications. Accessed June 20, 2024. Https://www.Usmint.Gov/learn/coin-and-medal-programs/coin-specifications.
22. Manohara SR, Hanagodimath SM, Thind KS, Gerward L. On the effective atomic number and electron density: A comprehensive set of formulas for all types of materials and energies above 1 keV. *Nucl Instrum Methods Phys Res B*. 2008;266:3906-3912.
23. SI Metric. Specific gravity of metals. Accessed June 20, 2024. https://www.simetric.co.uk/si_metals.htm.